

Solution-Processable Dithienothiophenoquinoid (DTTQ) Structures for Ambient-Stable n-Channel Organic Field Effect Transistors

Sureshraj V. Vegiraju, Guan-Yu He, Choongik Kim, Pragma Priyanka, Yen-Ju Chiu, Chiao-Wei Liu, Chu-Yun Huang, Jen-Shyang Ni, Ya-Wen Wu, Zhihua Chen, Gene-Hsiang Lee, Shih-Huang Tung, Cheng-Liang Liu,* Ming-Chou Chen,* and Antonio Facchetti*

A series of dialkylated dithienothiophenoquinoids (DTTQs), end-functionalized with dicyanomethylene units and substituted with different alkyl chains, are synthesized and characterized. Facile one-pot synthesis of the dialkylated DTT core is achieved, which enables the efficient realization of DTTQs as n-type active semiconductors for solution-processable organic field effect transistors (OFETs). The molecular structure of hexyl substituted DTTQ-6 is determined via single-crystal X-ray diffraction, revealing DTTQ is a very planar core. The DTTQ cores form a “zig-zag” linking layer and the layers stack in a “face-to-face” arrangement. The very planar core structure, short core stacking distance (3.30 Å), short intermolecular S–N distance (2.84 Å), and very low lying lowest unoccupied molecular orbital energy level of –4.2 eV suggest that DTTQs should be excellent electron transport candidates. The physical and electrochemical properties as well as OFETs performance and thin film morphologies of these new DTTQs are systematically studied. Using a solution-shearing method, DTTQ-11 exhibits n-channel transport with the highest mobility of up to $0.45 \text{ cm}^2 \text{ V}^{-1} \text{ s}^{-1}$ and a current ON/OFF ratio ($I_{\text{ON}}/I_{\text{OFF}}$) greater than 10^5 . As such, DTTQ-11 has the highest electron mobility of any DTT-based small molecule semiconductors yet discovered combined with excellent ambient stability. Within this family, carrier mobility magnitudes are correlated with the alkyl chain length of the side chain substituents of DTTQs.

1. Introduction

Organic small molecular semiconductors have attracted much attention for their potential applications in organic field effect transistors (OFETs) for memory devices, smart cards, radio frequency identification tags, electronic papers, flexible displays, and sensors.^[1–9] Among these, solution-processable small molecules with high performance and ambient stability are of great interest due to their possibility of a low-cost solution process and high flexibility in molecular design/modification for various OFETs applications.^[10–17] The molecular design of these semiconductors include aromatic building blocks with good π -conjugation for optimal charge transport and appropriate alkyl chain substitution to enable processability. With regard to the conjugated heterocyclic aromatics, fused- and oligothiophenes are extensively studied in OFETs due to their extensive conjugation, strong intermolecular S–S interactions, highly coplanar

Dr. S. Vegiraju, Dr. P. Priyanka, Y.-J. Chiu, C.-W. Liu,
C.-Y. Huang, Y.-W. Wu, Prof. M.-C. Chen
Department of Chemistry
National Central University
Taoyuan 32001, Taiwan
E-mail: mcchen@ncu.edu.tw

G.-Y. He, Prof. C.-L. Liu
Department of Chemical and Materials Engineering
National Central University
Taoyuan 32001, Taiwan
E-mail: clliu@ncu.edu.tw

Prof. C. Kim
Department of Chemical and Biomolecular Engineering
Sogang University
Seoul 121742, South Korea

Dr. J.-S. Ni
Institute of Chemistry
Academia Sinica
Taipei 11529, Taiwan

Z. Chen, Prof. A. Facchetti
Polyera Corporation
Skokie, IL 60077, USA
E-mail: a-facchetti@northwestern.edu

G.-H. Lee
Instrumentation Center
National Taiwan University
Taipei 10617, Taiwan

Prof. S.-H. Tung
Institute of Polymer Science and Engineering
National Taiwan University
Taipei 10617, Taiwan

Prof. A. Facchetti
Department of Chemistry and the Materials Research Center
Northwestern University
Evanston, IL 60208, USA

DOI: 10.1002/adfm.201606761

cores, and higher ambient stabilities.^[18–20] In particular, fused thiophenes exhibit a planar backbone structure and strong π - π stacking in the solid state, resulting in the enhancement of the neighboring molecular orbital overlapping, and so enabling more efficient charge carrier transport. As a result, a variety of small molecular and polymeric fused thiophene semiconductors have been reported.^[21–28] However, solution-processable fused thiophenes remain relatively unexplored compared to other π -conjugated systems. We are particularly interested in small molecules, since the latter have a number of advantages over polymers, such as structural versatility, facile synthesis, high purity, better reproducibility, and reliability without batch-to-batch variations. Alkyl chain modifications such as changing their length, installing branched alkyl side chains, and altering the positions of branches will help to achieve high device performance in solution-processable small molecules.^[27,29–34] All of these factors strongly direct the molecular packing and intermolecular interactions of the organic semiconductors.

The development of solution-processable n-type materials has lagged behind that of the related p-type materials. It is not until recently that solution-processed tetraazapentacene semiconductors exhibited high n-channel mobility up to $11 \text{ cm}^2 \text{ V}^{-1} \text{ s}^{-1}$ at room temperature.^[35,36] Unlike pentacene-based semiconductors, the development of solution-processable fused thiophene based n-type materials are much rare and exhibit lower mobilities than their p-type counterparts.^[20,37,38] Among the reported n-type fused and oligothiophene containing compounds, dicyanomethylene substituted quinoidal molecules are interesting n-type materials due to their low-lying lowest unoccupied molecular orbital (LUMO) and strong electron affinity.^[39,40] A few noteworthy examples of the studied oligothiophenoidal organic n-channel semiconductors are shown in **Figure 1**. Vacuum deposited films of the oligothiophene **DCMT (I)** were reported with an OFETs electron mobility of up to $0.20 \text{ cm}^2 \text{ V}^{-1} \text{ s}^{-1}$.^[41] When thienoquinoidal compounds **(II)**^[42] and **TTTCN (III)**^[10,43] were deposited from solution, the corresponding OFETs achieved electron mobilities of $0.16 \text{ cm}^2 \text{ V}^{-1} \text{ s}^{-1}$ and $0.05 \text{ cm}^2 \text{ V}^{-1} \text{ s}^{-1}$, respectively, whereas the (alkyloxycarbonyl)cyanomethylene terthiophene **3T (IV)** quinoid structure processed similarly to the latter's exhibited an electron mobility of $0.015 \text{ cm}^2 \text{ V}^{-1} \text{ s}^{-1}$.^[1] Note that OFETs performance of quinoidal oligothiophenes processed either by vacuum or solution processes are consistently lower compared to those of quinoidal fused thiophenes. For example, the electron mobilities of the two **(V)** and four **(VI)** ring-fused thienoquinoids are as high as 0.22 and $0.90 \text{ cm}^2 \text{ V}^{-1} \text{ s}^{-1}$, respectively.^[12,44,45]

Dithieno[3,2-*b*:2',3'-*d*]thiophene (DTT) units are one of the promising building blocks of conjugated materials and exhibit decent p- and n-channel charge carrier mobilities in OFETs.^[18,46,47] However, most DTTs were examined

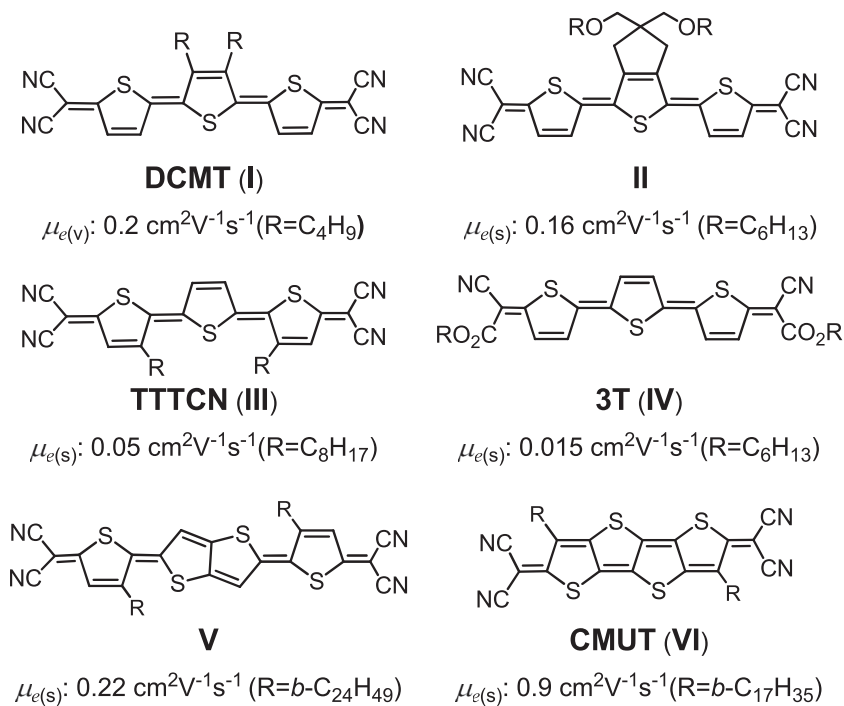
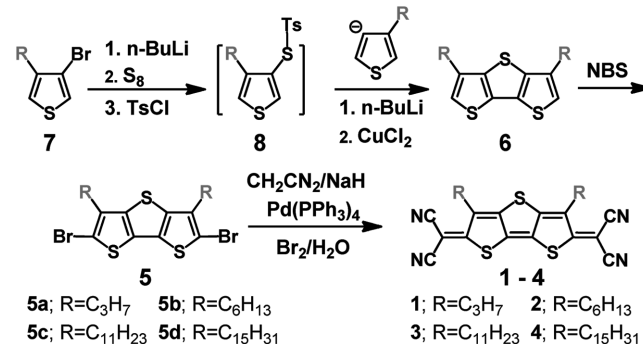


Figure 1. Chemical structures and OFET performances of the reported dicyanomethylene substituted thienoquinoidal n-type molecules. The symbols (v) and (s) denote vacuum and solution processed semiconductor films.

using vacuum deposition processes when implemented into OFETs.^[18,21,48,49] To date, the development of solution-processable organic semiconductors based on DTTs with tetracyano substituted thienoquinoid has not been reported for OFETs. In this work we explored and synthesized a series of dialkyl DTT-based dicyanomethylene end capped quinoids (**DTTQs, 1–4**, see **Scheme 1** for molecular structure) with various alkyl chains as solution-processable n-channel organic semiconductors. First, we explored a one-pot synthetic route for facile preparation of the dialkyl DTT core. Next, optical, electrochemical, and thermal characterization of these new **DTTQs** were performed and the results were compared. Furthermore, as revealed in the obtained crystal structure (vide infra), the newly developed **DTTQs** did exhibit a very planar structure, which enhanced molecular rigidity and π -polarization, thus resulting in a large π -conjugation with high film crystallinity for high device performance. Finally, organic semiconductor films were fabricated by



Scheme 1. Synthetic route to **DTTQ** compounds (**1–4**).

solution-shearing in a bottom-gate top-contact (BGTC) OFETs device architecture, and the electrical properties of resulting devices were characterized. Our results revealed that solution sheared thin films of **DTTQ-11** based OFETs exhibited excellent n-channel electrical performance, with a carrier mobility as high as $0.45 \text{ cm}^2 \text{ V}^{-1} \text{ s}^{-1}$ and a current ON/OFF ratio ($I_{\text{ON}}/I_{\text{OFF}}$) $> 10^5$. The **DTTQs** film morphologies and microstructures were characterized by polarized optical microscopy (POM), atomic force microscopy (AFM), and grazing incidence X-ray diffraction (GIXRD) to correlate with the device performances.

2. Results and Discussion

2.1. Synthesis

The chemical structures and synthesis of DTT-based thienoquinoids (**1–4**) are shown in Scheme 1. The Takahashi coupling reaction of the corresponding 2,6-dibromo-3,5-dialkyldithieno[3,2-*b*:2',3'-*d'*]-thiophene (**5a**, R = C₃H₇; **5b**, R = C₆H₁₃; **5c**, R = C₁₁H₂₃; **5d**, R = C₁₅H₃₁) with CH₂(CN)₂ was carried out in the presence of tetrakis(triphenylphosphine)palladium, followed by oxidation with saturated bromine water, and **DTTQs** (**1–4**) were obtained in a yield of 57%–68%. Dibrominated DTT (**5**) was prepared from the bromination of dialkylated DTT (**6**), which could be generated from 3-bromo-4-alkylthiophene (**7**) through stepwise procedures or via a one-pot synthetic route. For the one-pot methodology,^[20,46,47] compound **7** was first lithiated with *n*-BuLi, followed by the addition of S₈ and then TsCl to form the intermediate **8**. Without product purification, the mixture was treated with (4-alkylthiophen-3-yl)lithium, followed by a dilithiation with *n*-BuLi, and then ring closure by CuCl₂, to give the dialkyl DTT (**6**) in $\approx 30\%$ yield. Stepwise synthetic preparation of **6** was also achieved, as outlined in Scheme S3 of the Supporting Information, and the synthetic details are presented in the Supporting Information. Overall, the one-pot methodology provides a facile route for generation of **6**, while the stepwise procedure suffers tedious work-up along with longer acquired time. All the final quinoidal targets (**1–4**) possess the same central fused-thiophene DTT unit with varied alkyl chains of C₃H₇ (**1**; **DTTQ-3**), C₆H₁₃ (**2**; **DTTQ-6**), C₁₁H₂₃ (**3**; **DTTQ-11**), and C₁₅H₃₁ (**4**; **DTTQ-15**), and thus the solubility of these new **DTTQs** is high, and they are readily soluble in CH₂Cl₂, ethyl acetate, CHCl₃, toluene, and so on, at room temperature. In this series, the propylated **DTTQ-3** has

the lowest solubility and undecanoylated **DTTQ-11** possesses the highest solubility. Pentadecanoylated **DTTQ-15** exhibits lower solubility compared to **DTTQ-11**, which is probably due to the intermolecular interactions between long alkyl chains, similar to previously reported results.^[50–52] With the suitable alkyl chain length installed into the side position of quinoidal DTT core, it can provide adequate solubility for solution-processing of the organic semiconductor thin film and does not disrupt the π - π intermolecular interactions. Thus, more favorable film morphology from the ordered molecular assembly can be developed to facilitate charge carrier transport, as discussed later.

2.2. Physical Characterization

Thermal analyses of these new organic semiconductors were performed using differential scanning calorimetry (DSC) and thermogravimetric analysis (TGA; Figure S1, Supporting Information), and the corresponding thermal data are summarized in Table 1. As revealed in DSC scans, all four **DTTQs** possess high melting points with sharp endotherms above 194 °C. From the TGA measurement, it can be seen that all four molecules exhibited high thermal stability with 5% weight loss at temperatures up to 355 °C (under nitrogen). The shortest propyl **DTTQ-3** exhibits the highest thermal stability above 390 °C. It is interesting to note that the thermal decomposition of four **DTTQs** all occurred from the two connected alkyl chains breaking, as confirmed from their TGA weight loss percentages.

The UV-vis absorption spectra of both in *o*-dichlorobenzene and films prepared from solution-shearing are shown in Figure 2. As seen in Figure 2a, all the solution state absorption spectra are almost identical, and exhibit maximum absorption wavelengths (λ_{max}) at $\approx 555 \text{ nm}$, suggesting that variations in alkyl chain length do not have strong influences on the π -conjugated dithienothiophene backbone.^[40,45] However, the absorption spectra of the **DTTQ** solution-sheared films become broader, which can be explained by aggregation (Figure 2b). The energy gap derived from the absorption edge is 1.82–1.84 eV, as summarized in Table 1. All these solution-sheared films have blue-shifted λ_{max} of about 64–73 nm in comparison with their absorption in solution, indicating an H-type intermolecular aggregation of **DTTQ** molecules in the solid state.^[40] The origin of this strong aggregation tendency may be traced back to their inherently planar structures (vide infra). Because of the

Table 1. Thermal, optical, and electrochemical properties of **DTTQs**.

Compound	$T_{\text{d}}^{\text{a)}$ [°C]	$T_{\text{m}}^{\text{b)}$ [°C]	$\lambda_{\text{abs}}(\text{soln})^{\text{c)}$ [nm]	$\lambda_{\text{abs}}(\text{film})^{\text{d)}$ [nm]	$\Delta E_{\text{g}}(\text{opt})^{\text{e)}$ [eV]	$E_{\text{ox}}^{\text{f)}$ [V]	HOMO ^{g)} [eV]	$E_{\text{red}}^{\text{f)}$ [V]	LUMO ^{g)} [eV]	$\Delta E_{\text{g}}(\text{DPV})^{\text{h)}$ [eV]
DTTQ-3	390	209	525 555	491 626	1.82	1.92	-6.12	0.01	-4.21	1.91
DTTQ-6	362	208	525 555	483 651	1.83	1.93	-6.13	0.02	-4.22	1.91
DTTQ-11	355	194	525 555	482 651	1.84	1.96	-6.16	0.01	-4.21	1.95
DTTQ-15	359	197	525 555	487 651	1.84	1.96	-6.16	0.01	-4.21	1.95

^{a)}Decomposition temperatures were determined from TGA; ^{b)}Melting temperatures were determined from DSC; ^{c)}Absorption spectra were measured in *o*-C₆H₄Cl₂; ^{d)}Thin films were solution-sheared onto a quartz glass; ^{e)}The thin film optical energy gap was calculated using $1240/\lambda_{\text{abs}}(\text{onset})$; ^{f)}By DPV in *o*-C₆H₄Cl₂ at 25 °C. All potentials are reported with reference to an Fc+/Fc internal standard (at +0.6 V); ^{g)}Using HOMO/LUMO = $-(4.2 + E_{\text{ox}}/E_{\text{red}})$; ^{h)}The energy gap was calculated from the difference between HOMO and LUMO measured by DPV.

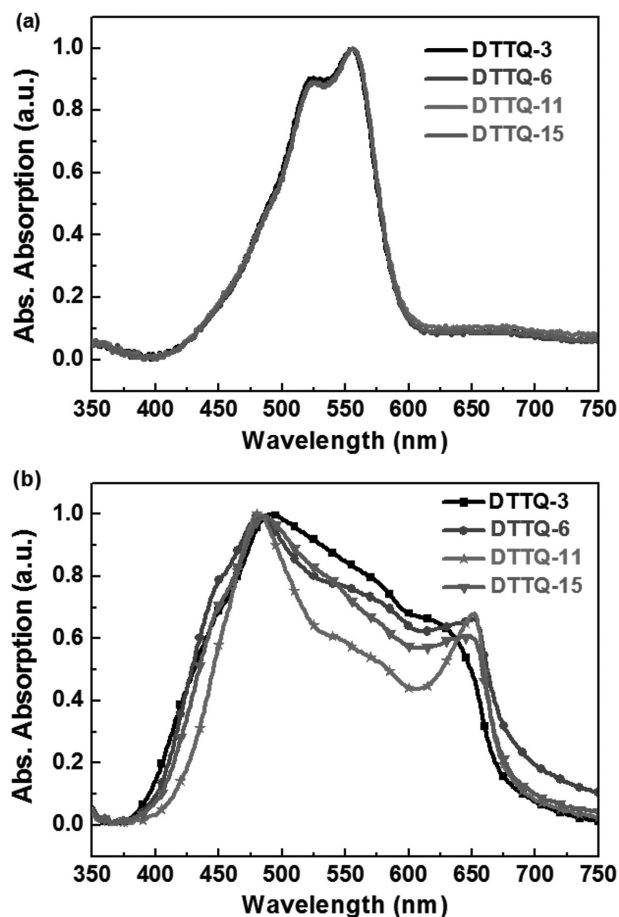


Figure 2. UV-visible spectra of DTTQs in a) *o*-dichlorobenzene and b) solution-sheared film state.

Davydov splitting due to aggregation, the absorption shoulder/band in the solid state optical spectra at a relatively longer wavelength (626 nm for DTTQ-3 and 651 nm for all other samples) corresponds to the low energy transition. In particular, the higher intensity in this absorption band for DTTQ-11 may be evidence for the stronger intermolecular interactions for this π -system. These spectral changes in the DTTQs thin films confirm that molecular packing of solution-sheared thin films can be significantly influenced by the length of the alky side chain.

The electrochemical properties were examined by differential pulse voltammetry (DPV) in *o*-dichlorobenzene with a 0.1 M Bu_4NPF_6 solution at 25 °C. The oxidation and reduction potential curves are shown in Figure 3a, and the corresponding data are summarized in Table 1. The DPV data show that all the quinoids possess similar oxidation and reduction potentials, and thus there is no significant alkyl chain effect on the electrochemical properties of the DTTQs. DPVs of the reduction and oxidation peaks of four DTTQs are exhibited at 0.01 and 1.94 V, respectively, while Fc/Fc^+ was used as an internal

standard calibrated at +0.60 eV. Consequently, the derived LUMO and the highest occupied molecular orbital (HOMO) of 1–4 are estimated at around -4.21 and -6.14 eV, respectively, according to the equation: $\text{HOMO}/\text{LUMO} = -(4.2 + E_{\text{ox}}/E_{\text{red}})$; assuming ferrocene/ferrocenium oxidation at -4.8 eV. Accordingly, the electrochemically derived HOMO–LUMO energy gaps of four DTTQs are ≈ 1.95 eV. As shown in Figure 3b, the HOMO energy levels of DTTQs are downshifted compared to that of CMUT (IV; Figure 1, four ring-fused thienoquinoid), due to reduced number of π electrons. Nevertheless, the LUMO energies of these newly developed DTTQs are all below -4.1 eV, therefore, the DTT-based quinoids are potentially environmentally stable n-channel semiconductors for OFETs.^[53]

2.3. Molecular Orbital Computations

Electronic structure calculations were performed at the B3LYP/6-31G* level of density functional theory (DFT) to evaluate the frontier molecular orbitals of DTTQ compounds. The alkyloxy carbonyl cyanomethylene moiety (1a) was also calculated to compare the electron withdrawing abilities of the dicyanomethylene versus the alkyloxy carbonyl cyanomethylene moieties. From the theoretical calculations, all four compounds have similar electron density HOMO and LUMO distributions; the electron densities are delocalized on the whole conjugated unit. The calculated HOMO (-6.26 eV) and LUMO (-4.18 eV) energy levels of DTTQ compounds are consistent with the optical absorption and DPV data, and are significantly down shifted compared to those of 1a (HOMO of -5.89 eV and LUMO of -3.80 eV; Figure S2, Supporting Information), which indicates the stronger electron withdrawing nature of the cyano group than the ester group. The calculated LUMO of dicyanomethylenyl DTTQs are all below -4.1 eV, in contrast, the LUMO of monocyanomethylenyl DTTQ (-3.80 eV; 1a) is still above -4.1 eV, indicating only the dicyanomethylenyl DTT quinoids are potentially environmentally stable OFETs.^[54–57]

2.4. Crystal Structure

Single crystals of DTTQ-6 were obtained from hexanes and dichloromethane solvent mixture by slow solvent evaporation. The diffraction-derived single-crystal structure of DTTQ-6,

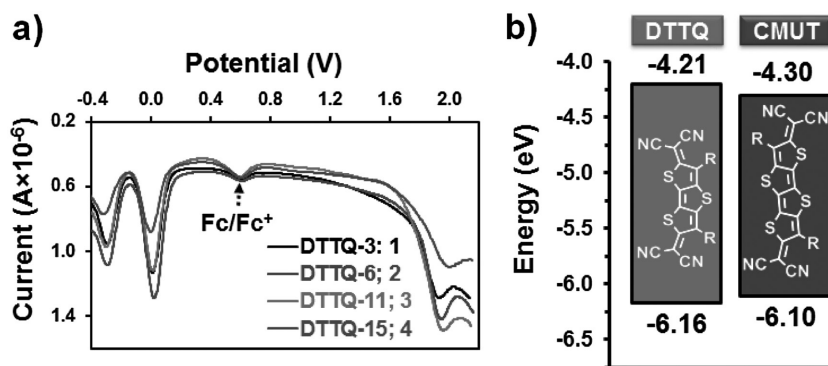


Figure 3. a) DPV of DTTQs in *o*-dichlorobenzene. b) DPV-derived HOMO and LUMO energy levels.

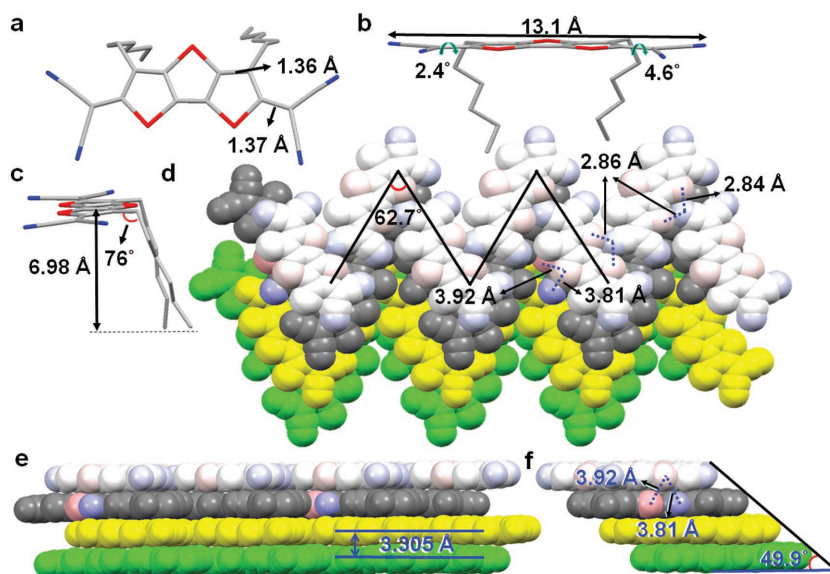


Figure 4. Single crystal structure of **DTTQ-6** in a–c) stick and d–f) space filling models. a,d) top view; b,e) front view; c,f) side view. a) **DTTQ-6** with molecular length of 13.1 Å. b) The **DTTQ** main core is very planar. The CN end-capping group planes to the **DTTQ** central plane with small dihedral angles of 4.6° and 2.4°. c) The two hexyl chains are paired on the same core face with an average out bending angle of 76°. d) The zig-zag angle between two neighboring **DTTQ** cores is 62.7°. e) **DTTQ** cores pack with face-to-face stacking and with a layer distance of 3.305 Å. f) **DTTQ** packing viewed along a π -plane direction (short axis) exhibits the layer slipping angle of 49.9°. Among the **DTTQ** layers, the shortest intermolecular S–N distance is 2.84 Å. In the **DTTQ** stacking, the interlayer S–N and S–S distances are 3.82 and 3.92 Å.

as the representative of this family, is shown in **Figure 4**, and detailed crystal structure data are summarized in Table S1 (Supporting Information). As shown in **Figure 4**, **DTTQ-6** recrystallizes in the monoclinic space group of $P 2_1/c$. Both CN-capped methylene end groups to the DTT core have an average C–C distance of 1.37 Å, exhibiting the characteristic of a double bond (**Figure 4a**). The **DTTQ** main core and the two end-capped CN groups are nearly coplanar, with small torsion angles of 2.4°–4.6° (**Figure 4b**). The two hexyl chains are located on the same DTT core face with a bending angle of 76° out of the **DTTQ** core (**Figure 4c**). The **DTTQ** molecules are linked in a “zig-zag” connection layers and the layers exhibit a slipped “face-to-face” packing arrangement (**Figure 4d**). In each layer, the “zig-zag” angle between two neighboring **DTTQ** cores is 62.7° and the DTT cores are connected by the closely adjacent S–N contacts with the shortest intermolecular S–N distance of 2.84 Å (**Figure 4d** and **Figure S3a**, Supporting Information). Among each layering stack, the **DTTQ** cores are spaced at a distance of 3.305 Å (**Figure 4e**) and possess interlayer S–N and S–S distances of 3.82 and 3.92 Å, respectively (**Figure 4f** and **Figure S3a**, Supporting Information). Viewed along the short axis π -plane direction, **DTTQ** exhibits a layer slipping angle of 49.9° (**Figure 4f**). In summary, the planar molecular structure, short main-core stacking distance (3.30 Å), and short intermolecular S–N distance (2.84 Å) of **DTTQ** suggest ideal conditions for the extended π -orbital interaction of the corresponding molecule, resulting in decent device performance (vide infra). The charge transport in this packing structure can be achieved either through face-to-face parallel molecules in the same stack, or through the well “zig-zag” connected neighboring molecules.

2.5. Charge Transport Measurements

The effects of alkyl substituent length in the side chain of **DTTQ** derivatives on the organic semiconductor performance were explored by fabricating OFETs. The organic semiconducting layer was fabricated by the solution-shearing method since the thin film morphology can be optimized by varying several processing parameters such as shearing speed, semiconductor concentration, and the substrate temperature as well as the crystalline semiconductor domains can be potentially aligned with the shearing force.^[58–62] OFETs device fabrication and measurement details are reported in the Experimental Section. All OFETs were processed in ambient atmosphere and tested both in an N_2 -filled box and ambient conditions, providing similar characteristics. Certain devices were stored in the air for further ambient stability measurements. The HOMO and LUMO levels of **DTTQ** compounds, which are almost independent of the core functionalization, are suitable for electron transport with good injection from Ag contacts. Furthermore, the aligned and crystalline solution-sheared thin films may enable good charge transport. Representative electrical character-

istics of the **DTTQ** series compounds as channel semiconductors are presented in **Figure 5**. The transfer characteristic (drain current–gate voltage; I_d – V_g) in **Figure 5a** exhibit a predominant n-type behavior, whereas the output characteristic (drain current–drain voltage; I_d – V_d) of same device with V_g ranging from 0 to 100 V present an unambiguous current saturation that is typical for good performing OFETs, as shown in **Figure 5b–e**. All the **DTTQ** OFETs exhibit similar electron transport characteristics in air and under N_2 atmosphere, suggesting good stability in both conditions. The charge carrier mobility (μ) and threshold voltage (V_{th}) are calculated from the slope and intercept of the square root of I_d versus V_g according to the standard saturation region, respectively. Detailed statistical calculations of the device performance metrics, including maximum mobility (μ_{max}), average mobility (μ_{avg}), V_{th} , I_{ON}/I_{OFF} obtained from over ten devices, are summarized in **Table 2**.

As can be seen from the field effect mobility for the device fabricated from series of small molecule semiconductors, the results showed the nonmonotonic dependency on the field effect mobility versus the alkyl chain length. The corresponding **DTTQ** derivatives show an increasing mobility trend, with the highest mobility of around $0.45 \text{ cm}^2 \text{ V}^{-1} \text{ s}^{-1}$ and average mobility of $0.29 \pm 0.09 \text{ cm}^2 \text{ V}^{-1} \text{ s}^{-1}$ observed in **DTTQ-11**, as the length of the alkyl side chain substituent increases from 3 to 6 and 11 carbons. On the other hand, a ten-time decrease in mobility ($0.029 \text{ cm}^2 \text{ V}^{-1} \text{ s}^{-1}$ in maximum and $0.021 \pm 0.007 \text{ cm}^2 \text{ V}^{-1} \text{ s}^{-1}$ in average) was observed for **DTTQ-15** with the longest alky chains. The I_{ON}/I_{OFF} is typically greater than 10^4 for this series of **DTTQ**s. Electrical hysteresis of solution-sheared n-type OFETs can be easily found during the dual

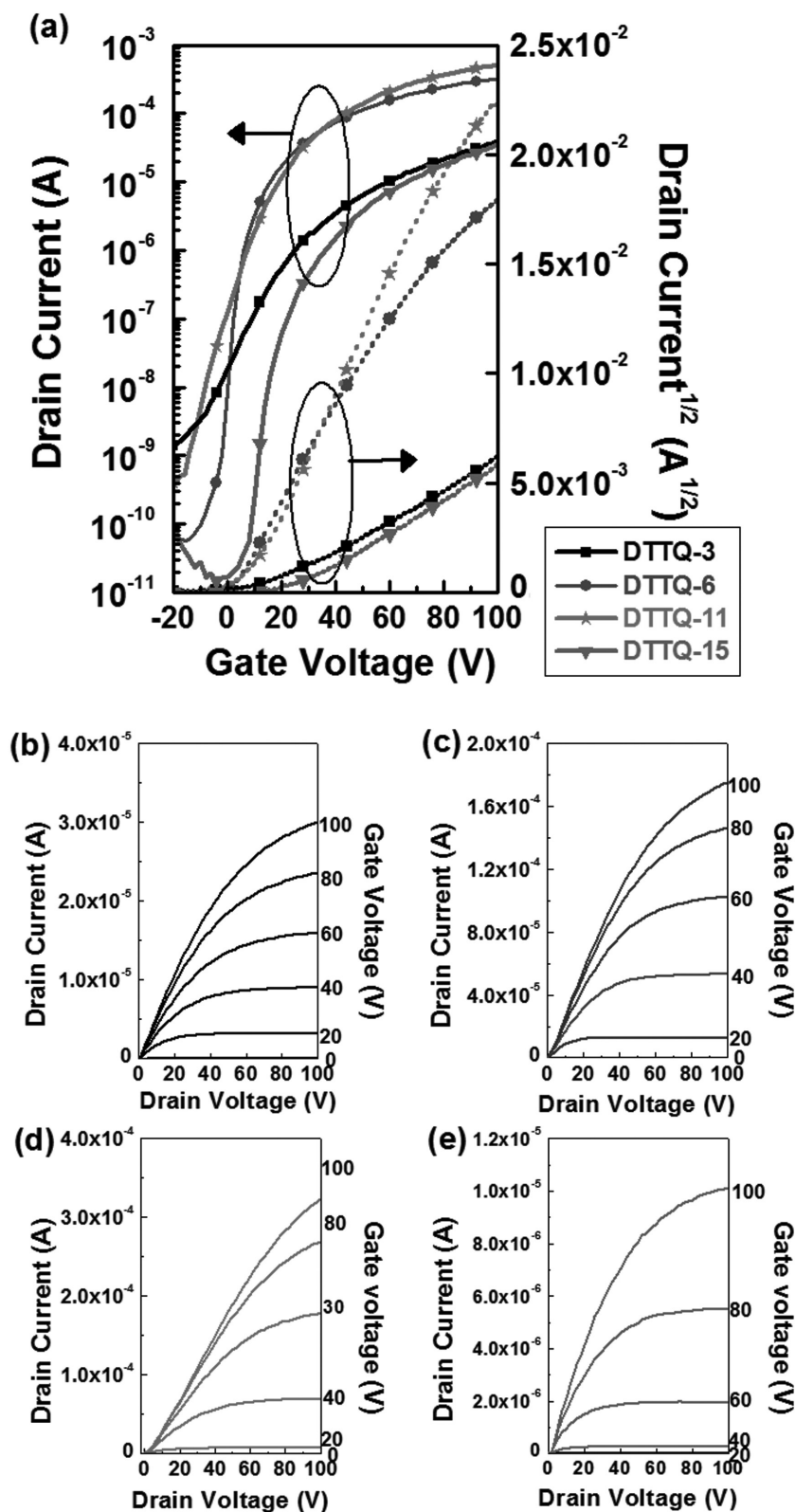


Figure 5. Transfer characteristics of solution-sheared OFETs based on a) DTTQ thin films. Output characteristics of solution-sheared OFETs based on b) DTTQ-3, c) DTTQ-6, d) DTTQ-11, and e) DTTQ-15 thin films. All the OFETs were measured in air at room temperature.

sweep scans.^[63] Similar phenomena were also recorded in our solution-sheared DTTQ OFETs (see Figure S4, Supporting Information) mainly due to the charge trapping in the interface between the DTTQs and dielectric interface or inside the DTTQs semiconducting channel (may be provided by rough solution-sheared surface). Furthermore, control DTTQ OFETs fabricated by depositing the semiconductor by traditional spin-coating technique were also prepared in order to evaluate and compare the charge transport properties. The representative transfer curves of spin-coated devices are shown in Figure S5 (Supporting Information). The extracted electron mobilities of the spin-coated DTTQ OFETs were over one order of magnitude lower than the solution-sheared ones, and correlated to the resulting morphology of the active layer, as will be discussed latter. Among all the OFETs produced with spin-coating, DTTQ-6 had a maximum mobility of $0.029 \text{ cm}^2 \text{ V}^{-1} \text{ s}^{-1}$, as summarized in Table 2.

2.6. Thin Film Microstructural Characterization and Correlation to Charge Transport

To obtain a better understanding of the impact of the alkyl chain length on the OFETs performance, the thin film morphologies and molecular packing structures were investigated by POM (Figure 6), AFM (Figure 7), and GIXRD (Figure 8) in which the fabricated thin film conditions are identical to those used for OFETs measurements. Figure 6 shows the POM of solution-sheared DTTQ films under the cross polarized light and all exhibit strong birefringence featuring elongated crystalline domains along the shearing direction. It is worth noting that the solution-shearing process was used to deposit DTTQ thin films as the semiconducting channel materials throughout the whole substrate. Directional stripe domains originated from multiple nucleation points can be clearly observed and quasi one-directional continuous crystals with stacks of crystalline plates are noticeable for the films of DTTQ-6 and DTTQ-11. However, in the case of DTTQ-15, the limited elongated grain generates visible boundaries that negatively affected charge transport (vide supra).

AFM topographic images of solution-sheared DTTQ-6, DTTQ-11, and DTTQ-15 exhibit terrace-like morphologies (Figure 7b-d). In particular, slow deposition of DTTQ-11 crystals due to the unidirectional

Table 2. Summary of OFETs parameters based on solution-sheared and spin-coated DTTQ thin films, as measured in air at room temperature.

Compound	Solution-sheared film				Spin-coated film			
	$\mu_{\max}^a)$ [cm ² V ⁻¹ s ⁻¹]	$\mu_{\text{avg}}^b)$ [cm ² V ⁻¹ s ⁻¹]	$V_{\text{th}}^b)$ [V]	$I_{\text{ON}}/I_{\text{OFF}}$ [-]	$\mu_{\max}^a)$ [cm ² V ⁻¹ s ⁻¹]	$\mu_{\text{avg}}^b)$ [cm ² V ⁻¹ s ⁻¹]	$V_{\text{th}}^b)$ [V]	$I_{\text{ON}}/I_{\text{OFF}}$ [-]
DTTQ-3	0.025	0.023 ± 0.002	9.2 ± 2.0	10 ³ –10 ⁴	0.0008	0.0004 ± 0.0003	9.2 ± 2.0	10 ³ –10 ⁴
DTTQ-6	0.27	0.22 ± 0.03	3.2 ± 3.0	10 ⁵ –10 ⁷	0.029	0.023 ± 0.005	–6.5 ± 0.5	10 ⁵ –10 ⁶
DTTQ-11	0.45	0.29 ± 0.09	6.4 ± 7.0	10 ⁴ –10 ⁵	0.013	0.012 ± 0.005	4.5 ± 2.0	10 ⁵ –10 ⁶
DTTQ-15	0.029	0.021 ± 0.007	2.3 ± 5.3	10 ⁴ –10 ⁵	0.005	0.003 ± 0.002	17.8 ± 8.4	10 ⁴ –10 ⁵

^{a)}Maximum mobility; ^{b)}The average TFT characteristics were obtained from more than ten devices originating from three to four semiconductor depositions.

shearing force forms connected and relatively smooth domains, with a typical roughness of 2.4 nm. Due to the limited solubility of the shorter alkyl side chain on the DTTQ-3, the inter-grain boundary and surface roughness increase with scattered small aggregates (≈12.8 nm), as shown in Figure 7a, consistent with a decreased electron mobility. Besides, longer insulating side chain substituents in the DTTQ-15 compound may limit the charge transport and thus negatively affect the field effect mobility, although it can also grow a highly oriented crystalline film.

On the other hand, the variation in mobility between the solution-sheared and spin-coated OFETs agrees well with morphological changes observed in the DTTQ films. Spin-coated DTTQ films prepared on a (2-phenylethyl)trichlorosilane (PETS)-modified Si/SiO₂ substrates form plate-like crystals with a much smaller crystalline size (see POM and AFM in Figures S6 and S7, respectively, of the Supporting Information), which agrees with a fast film growth process in the DTTQ films and a lower mobility value. Regardless of the film fabrication methods used, these results indicate that the improved performances of spin-coated OFETs based on DTTQ-6 and DTTQ-11 as compared to DTTQ-3 and DTTQ-15 are mainly due to an increase in interconnected aggregates on a micrometer length scale, even though these aggregates are small when compared to those found in the solution-sheared highly crystalline DTTQ films.

2D GIXRD experiments were also performed on the solution-sheared DTTQ films with same preparation conditions

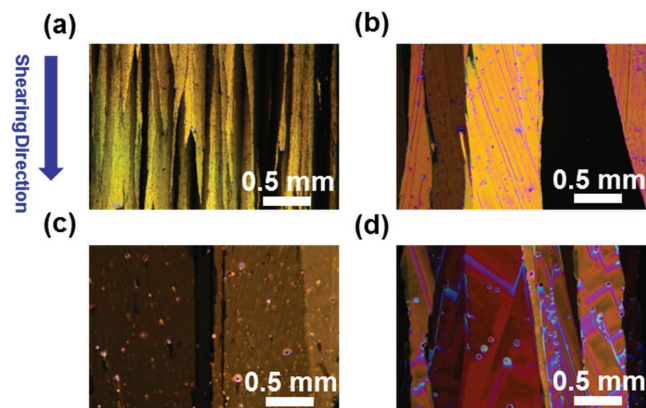


Figure 6. POM image of solution-sheared a) DTTQ-3, b) DTTQ-6, c) DTTQ-11, and d) DTTQ-15 thin films.

relative to the OFETs devices (see Figure 8). All the DTTQ films display intense reflections, indicating the presence of crystalline domains. The lattice parameters of solution-sheared DTTQ crystals, as deduced from Figure 8, show that the a (001) interlayer distance (d_{001} -spacing) along out-of-plane direction correlates with the separation of the π -conjugated DTTQ backbone, which is directly related to the chain length of the alkyl substituents. Therefore, DTTQ-3 containing a propyl side chain shows the smallest d_{001} -spacing value of 13.0 Å, whereas DTTQ-6, DTTQ-11, and DTTQ-15 comprising longer hexyl, undecyl, and pentadecyl side chains, give longer values of 17.7, 22.7, and 27.0 Å, respectively. The molecular packing of DTTQ-6 and DTTQ-11 is more ordered and oriented than that of DTTQ-3 and DTTQ-15, as determined from the sharper diffraction patterns. It can be concluded here that the side chain length attached to the central conjugated core is critical to the morphologies and crystalline structures in solution-processed thin films. The well-oriented crystalline stripes that are over a centimeter long, extensive intermolecular packing interaction, and higher degree of inter chain ordering in the resulting DTTQ-6 and DTTQ-11 films, are essential to enhancing device performance.

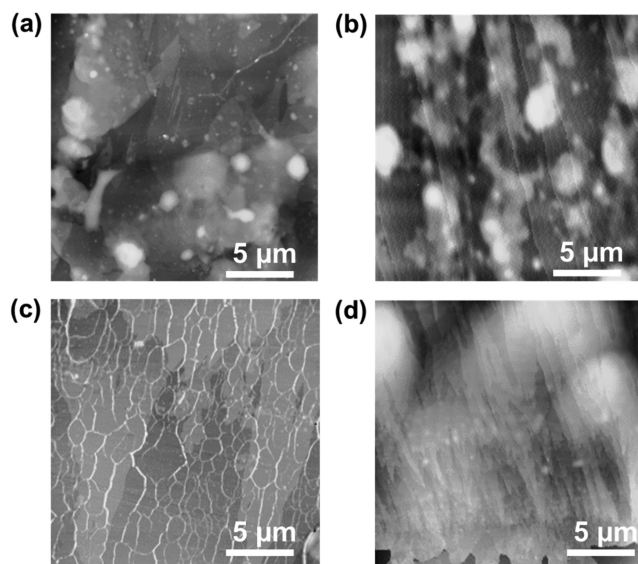


Figure 7. AFM image of solution-sheared a) DTTQ-3, b) DTTQ-6, c) DTTQ-11, and d) DTTQ-15 thin films on the PETS-treated Si/SiO₂ substrate.

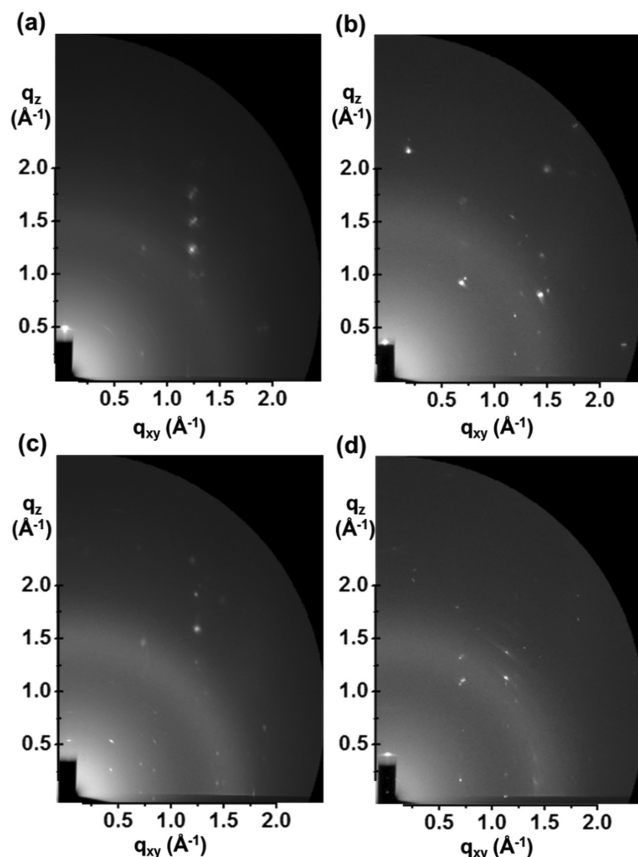


Figure 8. 2D GIXRD diffraction pattern images of solution-sheared a) DTTQ-3, b) DTTQ-6, c) DTTQ-11, and d) DTTQ-15 thin films.

2.7. Device Stability Measurements

To enable environmentally stable n-type semiconductors in ambient conditions it requires the conjugated core to be functionalized with strong electron-withdrawing groups so that to achieve an empirical LUMO energy below about -4.1 eV.^[53] Introducing four cyano groups at the end region of the DTTQ compounds lowers the LUMO level down to -4.2 eV, which could strongly improve the ambient stability of OFETs. Thus, we investigated the long-term environmental stability of DTTQ OFETs stored in ambient conditions (shelf storage without any electrical bias applied; at a relative humidity of 45%–55%). The mobility versus time plots of **Figure 9** demonstrate that these non-encapsulated/non-passivated devices are quite stable throughout the whole exposure period. The stability of DTTQ-11 OFETs were further investigated by subjecting them to a continuous V_g sweeping (from -40 to 100 V) under a constant V_d of 100 V, as shown in Figure S8 (Supporting Information). After a series of 100 scans, the transfer curve almost overlaps the initial one and no performance degradation, including that of μ , V_{th} , and I_{ON}/I_{OFF} , can be observed. Therefore, the DTTQ compound can enable transport states without significant trap-induced deterioration under the gate bias.

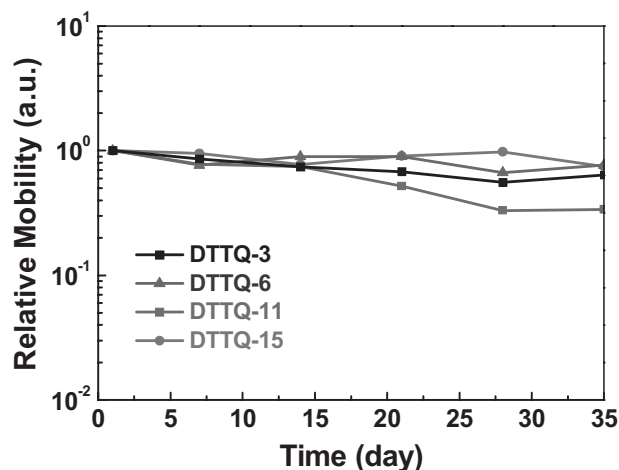


Figure 9. Long-term ambient stability of DTTQ OFETs based on Ag source and drain contacts, stored in ambient atmosphere.

3. Conclusions

Side chain structural variations on the semiconducting properties of a new quinoidal DTTQ small molecule series for OFETs have been investigated to establish molecular structure/processing/morphology/performance relationships. The combination of a proper solubility and molecular aggregation are important parameters to achieve well-connected large semiconductor domains with highly oriented molecular packing when processing the films for OFET applications. The use of the intermediate side chain lengths in DTTQ-6 and DTTQ-11 appears to be optimal for efficient charge transport, clearly outperforming the short and very long chains in DTTQ-3 and DTTQ-15, respectively. These observations are supported by optical absorption, microscopic image, and X-ray diffraction measurements. Among the newly developed quinoidal DTTQ derivatives, solution-sheared DTTQ-11 OFETs yield the highest mobility and exhibit good long-term ambient stability and electrical stability, thus making it attractive for use as a solution-processable n-type organic semiconductor based devices.

4. Experimental Section

Materials: All the chemical reagents were purchased from Aldrich, Alfa, and TCI Chemical Co. and used as received unless otherwise noted. Solvents for reactions (toluene and tetrahydrofuran (THF)) were distilled under nitrogen from sodium/benzophenone ketyl, and halogenated solvents were distilled from CaH_2 . Silane agent for the self-assembly monolayer (SAM) treatment, PETS or octadecyltrimethoxysilane (ODTS), was obtained from Gelest, Inc. Details for the preparation of dibrominated DTT (**5**) and one-pot or stepwise synthesis of dialkyl DTT (**6**; Scheme S2, Supporting Information) and 3-bromo-4-alkyl thiophene (**7**; Scheme S1, Supporting Information) were shown in the Supporting Information.

General Procedures for Final Target Compounds: Malononitrile (2.4 mmol) was added into a solution of sodium hydride (6.0 mmol) in dry dimethoxyethane (30 mL) at 0°C , and the mixture was warmed to room temperature and stirred for 30 min. 2,6-dibromo-3,5-dialkylidithieno[3,2-*b*:2',3'-*d*]-thiophene (**5**) (0.6 mmol) and tetrakis(triphenyl-phosphine)palladium (0.12 mmol) were then added. The mixture was refluxed for 12 h, and then saturated bromine water was added and stirred for 20 min. The mixture was extracted with

CH₂Cl₂, washed with brine, dried over Na₂SO₄ and evaporated. The residue was purified by column chromatography using ethyl acetate/hexanes followed by recrystallization from CH₂Cl₂/hexanes.

Synthesis of DTTQ-3(1): The title compound was obtained as a purple solid (yield = 46%). Mp: 209 °C. ¹H NMR (300 MHz, CDCl₃): δ 2.89 (t, *J* = 7.5 Hz, 4 H), 1.82–1.69 (m, 4 H), 0.71 (t, *J* = 7.2 Hz, 6 H). ¹³C NMR (125 MHz, CDCl₃): δ 170.78, 159.84, 136.44, 135.01, 113.48, 112.14, 72.75, 30.57, 22.98, 13.81. HRMS (*m/z* FAB+) calcd. for C₂₀H₁₄N₄S₃: 406.0381. Found: 406.0383.

Synthesis of DTTQ-6(2): The title compound was obtained as a purple solid (yield = 68%). Mp: 208 °C. ¹H NMR (300 MHz, CDCl₃): δ 2.90 (t, *J* = 7.5 Hz, 4 H), 1.74–1.64 (m, 4 H), 1.43–1.26 (br, 12 H), 0.90 (t, *J* = 6.9 Hz, 6 H). ¹³C NMR (75 MHz, CDCl₃): δ 170.77, 159.67, 136.71, 135.50, 113.52, 112.15, 72.67, 31.39, 29.48, 29.03, 28.85, 22.48, 14.00. HRMS (*m/z* FAB+) calcd. for C₂₆H₂₆N₄S₃: 490.1320. Found: 490.1323.

Synthesis of DTTQ-11(3): The title compound was obtained as a purple solid (yield = 57%). Mp: 194 °C. ¹H NMR (300 MHz, CDCl₃): δ 2.89 (t, *J* = 7.8 Hz, 4 H), 1.73–1.63 (m, 4 H), 1.42–1.25 (br, 32 H), 0.88 (t, *J* = 6.5 Hz, 6 H). ¹³C NMR (125 MHz, CDCl₃): δ 177.74, 159.64, 136.70, 134.96, 113.51, 112.14, 72.71, 31.90, 29.58, 29.52, 29.44, 29.37, 29.32, 29.27, 28.85, 22.69, 14.12. HRMS (*m/z* FAB+) calcd. for C₃₆H₄₆N₄S₃: 630.2885. Found: 630.2878.

Synthesis of DTTQ-15(4): The title compound was obtained as a purple solid (yield = 61%). Mp: 197 °C. ¹H NMR (300 MHz, CDCl₃): δ 2.90 (t, *J* = 7.5 Hz, 4 H), 1.72–1.64 (m, 4 H), 1.43–1.26 (br, 48 H), 0.88 (t, *J* = 6.3 Hz, 6 H). ¹³C NMR (125 MHz, CDCl₃): δ 170.71, 159.62, 136.70, 134.94, 113.49, 112.13, 72.76, 31.93, 29.67, 29.58, 29.53, 29.45, 29.37, 29.27, 28.85, 22.69, 14.12. HRMS (*m/z* FAB+) calcd. for C₄₄H₆₂N₄S₃: 742.4137. Found: 742.4132.

Characterization: ¹H and ¹³C NMR were recorded using a Bruker 500 or 300 instrument for all materials, with reference to solvent signals. Elemental analyses were performed on a Heraeus CHN-O-Rapid elemental analyzer. Mass spectrometric data were obtained with a JMS-700 HRMS instrument. DSC was carried out under a nitrogen atmosphere on a Mettler DSC 822 instrument (scanning rate of 10 °C min⁻¹). TGA was carried out using a Perkin Elmer TGA-7 thermal analysis system using dry nitrogen as a carrier gas at a flow rate of 10 mL min⁻¹ (heating rate of 10 °C min⁻¹), and the reported decomposition temperatures represent the temperature observed at 5% mass loss. DPV experiments were performed with a conventional three-electrode configuration (a platinum disk working electrode, an auxiliary platinum wire electrode, and a nonaqueous Ag reference electrode, with a supporting electrolyte of 0.1 M tetrabutylammonium hexafluorophosphate (TBAPF₆) in the specified dry solvent using a CHI621C Electrochemical Analyzer (CH Instruments). All electrochemical potentials were referenced to an Fc^{+/0}/Fc internal standard (at 0.6 V). The UV–vis spectrum was recorded on a Hitachi U-4100 UV–vis–NIR spectrophotometer. Polarized optical images were obtained with a Leica 2700M. The UV–vis spectrum was characterized with a JASCO V-670 UV–vis spectrophotometer. The thickness of the organic semiconductor thin films was measured with a DEKTA 150 Surface Profilometer (Veeco). AFM was performed in tapping mode at room temperature with a Seiko SPA400, for which NANOSENSORS Si tips with a resonant frequency of 160 kHz were used. GIXRD was carried out at room temperature on the beamline BL13A/BL17A in the National Synchrotron Radiation Research Center (NSRRC), Taiwan.

OFETs Device Fabrication and Characterization: The electrical semiconducting performance of the synthesized small molecules was carried out using BGTC OFET structures. Heavily n-doped Si wafers with 300 nm thermally oxidized SiO₂ dielectric were used as the substrates. The substrates were washed using an ultrasonic bath with acetone and isopropanol, and then treated with UV/ozone cleaner, prior to immersion in a solution of 5 × 10⁻³ M (PETS) in toluene kept at 50 °C for 90 min. Following PETS deposition, the substrates were sonicated with toluene and dried with an N₂ stream. All the DTTQ series compounds were stirred in chlorobenzene at 50 °C at a concentration of 2–5 mg mL⁻¹. Solution-shearing organic semiconductors thin films developed by Bao's group^[58–62] were prepared using a customized shearing machine, where

the upper shearing plate (modified with ODTS) dragged the placed solution (≈20 μL) on a heated substrate (50 °C) at a controlled shearing rate of 10–20 μm s⁻¹. On the other hand, spin-coated DTTQ films were also prepared for comparison (at a concentration of 5–10 mg mL⁻¹; spin rate of 2000 rpm for 60 s; annealing at 60 °C). The top source/drain electrode pairs with a channel length (*L*) of 20 μm and channel width (*W*) of 1500 μm were fabricated by thermal evaporation of Ag through the shadow mask, with the channel parallel to the shearing direction. All the electrical measurements were performed at room temperature inside an N₂-filled glove box and in air (relative humidity: 45%–55%), except for the study of ambient stability, which was performed in air, using a Keithley 4200-SCS semiconductor parameter analyzer.

Supporting Information

Supporting Information is available from the Wiley Online Library or from the author.

Acknowledgements

S.V. and G.-Y.H. contributed equally to this work. The authors acknowledge the financial support received from the Ministry of Science and Technology of Taiwan (MOST). The authors thank Beamline B13A1/B17A1 (National Synchrotron Radiation Research Center (NSRRC) of Taiwan) for providing beamtime. The discussion with Prof. Chien-Lung Wang of National Chiao Tung University and Dr. Chun-Jen Su of NSRRC is also highly appreciated.

Keywords

dithienothiophenes, n-type, organic field effect transistors, organic semiconductors, quinoids, solution-shearing

Received: December 22, 2016

Revised: February 17, 2017

Published online:

- [1] X. Guo, J. Quinn, Z. Chen, H. Usta, Y. Zheng, Y. Xia, J. W. Hennek, R. P. Ortiz, T. J. Marks, A. Facchetti, *J. Am. Chem. Soc.* **2013**, *135*, 1986.
- [2] A. N. Sokolov, M. E. Roberts, Z. Bao, *Mater. Today* **2009**, *12*, 12.
- [3] J. Zaumseil, H. Sirringhaus, *Chem. Rev.* **2007**, *107*, 1296.
- [4] Y. Mei, M. A. Loth, M. Payne, W. Zhang, J. Smith, C. S. Day, S. R. Parkin, M. Heeney, I. McCulloch, T. D. Anthopoulos, J. E. Anthony, O. D. Jurchescu, *Adv. Mater.* **2013**, *25*, 4352.
- [5] R. J. Kline, S. D. Hudson, X. Zhang, D. J. Gundlach, A. J. Moad, O. D. Jurchescu, T. N. Jackson, S. Subramanian, J. E. Anthony, M. F. Toney, L. J. Richter, *Chem. Mater.* **2011**, *23*, 1194.
- [6] N. A. Azarova, J. W. Owen, C. A. McLellan, M. A. Grimminger, E. K. Chapman, J. E. Anthony, O. D. Jurchescu, *Org. Electron.* **2010**, *11*, 1960.
- [7] J. L. Marshall, K. Uchida, C. K. Frederickson, C. Schutt, A. M. Zeidell, K. P. Goetz, T. W. Finn, K. Jarolimek, L. N. Zakharov, C. Risko, R. Herges, O. D. Jurchescu, M. M. Haley, *Chem. Sci.* **2016**, *7*, 5547.
- [8] A. Marrocchi, A. Facchetti, D. Lanari, C. Petrucci, L. Vaccaro, *Energy Environ. Sci.* **2016**, *9*, 763.
- [9] T. Erdmann, S. Fabiano, B. Milián-Medina, D. Hanifi, Z. Chen, M. Berggren, J. Gierschner, A. Salleo, A. Kiriy, B. Voit, A. Facchetti, *Adv. Mater.* **2016**, *28*, 9169.
- [10] S. R. Forrest, *Nature* **2004**, *428*, 911.
- [11] H. Yan, Z. Chen, Y. Zheng, C. Newman, J. R. Quinn, F. Dotz, M. Kastler, A. Facchetti, *Nature* **2009**, *457*, 679.

- [12] T. Sekitani, U. Zschieschang, H. Klauk, T. Someya, *Nat. Mater.* **2010**, *9*, 1015.
- [13] C. M. Lochner, Y. Khan, A. Pierre, A. C. Arias, *Nat. Commun.* **2014**, *5*, 5745.
- [14] S. L. Swisher, M. C. Lin, A. Liao, E. J. Leefflang, Y. Khan, F. J. Pavinatto, K. Mann, A. Naujokas, D. Young, S. Roy, M. R. Harrison, A. C. Arias, V. Subramanian, M. M. Maharbiz, *Nat. Commun.* **2015**, *6*, 6575.
- [15] A. Marrocchi, M. Seri, C. Kim, A. Facchetti, A. Taticchi, T. J. Marks, *Chem. Mater.* **2009**, *21*, 2592.
- [16] M. J. Sung, A. Luzio, W.-T. Park, R. Kim, E. Gann, F. Maddalena, G. Pace, Y. Xu, D. Natali, C. de Falco, L. Dang, C. R. McNeill, M. Caironi, Y.-Y. Noh, Y.-H. Kim, *Adv. Funct. Mater.* **2016**, *26*, 4984.
- [17] A. Luzio, D. Fazzi, F. Nübling, R. Matsidik, A. Straub, H. Komber, E. Giussani, S. E. Watkins, M. Barbatti, W. Thiel, E. Gann, L. Thomsen, C. R. McNeill, M. Caironi, M. Sommer, *Chem. Mater.* **2014**, *26*, 6233.
- [18] Y. M. Sun, Y. Q. Ma, Y. Q. Liu, Y. Y. Lin, Z. Y. Wang, Y. Wang, C. A. Di, K. Xiao, X. M. Chen, W. F. Qiu, B. Zhang, G. Yu, W. P. Hu, D. B. Zhu, *Adv. Funct. Mater.* **2006**, *16*, 426.
- [19] Y. Liu, Y. Wang, W. Wu, Y. Liu, H. Xi, L. Wang, W. Qiu, K. Lu, C. Du, G. Yu, *Adv. Funct. Mater.* **2009**, *19*, 772.
- [20] J. Youn, P.-Y. Huang, Y.-W. Huang, M.-C. Chen, Y.-J. Lin, H. Huang, R. P. Ortiz, C. Stern, M.-C. Chung, C.-Y. Feng, L.-H. Chen, A. Facchetti, T. J. Marks, *Adv. Funct. Mater.* **2012**, *22*, 48.
- [21] X.-C. Li, H. Sirringhaus, F. Garnier, A. B. Holmes, S. C. Moratti, N. Feeder, W. Clegg, S. J. Teat, R. H. Friend, *J. Am. Chem. Soc.* **1998**, *120*, 2206.
- [22] K. Xiao, Y. Liu, T. Qi, W. Zhang, F. Wang, J. Gao, W. Qiu, Y. Ma, G. Cui, S. Chen, X. Zhan, G. Yu, J. Qin, W. Hu, D. Zhu, *J. Am. Chem. Soc.* **2005**, *127*, 13281.
- [23] J. R. Matthews, W. Niu, A. Tandia, A. L. Wallace, J. Hu, W.-Y. Lee, G. Giri, S. C. B. Mannsfeld, Y. Xie, S. Cai, H. H. Fong, Z. Bao, M. He, *Chem. Mater.* **2013**, *25*, 782.
- [24] N. Zhou, S. Vegiraju, X. Yu, E. F. Manley, M. R. Butler, M. J. Leonardi, P. Guo, W. Zhao, Y. Hu, K. Prabakaran, R. P. H. Chang, M. A. Ratner, L. X. Chen, A. Facchetti, M.-C. Chen, T. J. Marks, *J. Mater. Chem. C* **2015**, *3*, 8932.
- [25] H. H. Fong, V. A. Pozdin, A. Amassian, G. G. Malliaras, D.-M. Smilgies, M. He, S. Gasper, F. Zhang, M. Sorensen, *J. Am. Chem. Soc.* **2008**, *130*, 13202.
- [26] J. Li, F. Qin, C. M. Li, Q. Bao, M. B. Chan-Park, W. Zhang, J. Qin, B. S. Ong, *Chem. Mater.* **2008**, *20*, 2057.
- [27] I. McCulloch, M. Heeney, C. Bailey, K. Genevicius, I. MacDonald, M. Shkunov, D. Sparrowe, S. Tierney, R. Wagner, W. Zhang, M. L. Chabynyc, R. J. Kline, M. D. McGehee, M. F. Toney, *Nat. Mater.* **2006**, *5*, 328.
- [28] N. Zhou, K. Prabakaran, B. Lee, S. H. Chang, B. Harutyunyan, P. Guo, M. R. Butler, A. Timalisina, M. J. Bedzyk, M. A. Ratner, S. Vegiraju, S. Yau, C.-G. Wu, R. P. H. Chang, A. Facchetti, M.-C. Chen, T. J. Marks, *J. Am. Chem. Soc.* **2015**, *137*, 4414.
- [29] J. Lee, A. R. Han, H. Yu, T. J. Shin, C. Yang, J. H. Oh, *J. Am. Chem. Soc.* **2013**, *135*, 9540.
- [30] H. Chen, Y. Guo, G. Yu, Y. Zhao, J. Zhang, D. Gao, H. Liu, Y. Liu, *Adv. Mater.* **2012**, *24*, 4618.
- [31] I. Osaka, R. Zhang, G. Sauvé, D.-M. Smilgies, T. Kowalewski, R. D. McCullough, *J. Am. Chem. Soc.* **2009**, *131*, 2521.
- [32] C. Wang, Y. Qin, Y. Sun, Y.-S. Guan, W. Xu, D. Zhu, *ACS Appl. Mater. Interfaces* **2015**, *7*, 15978.
- [33] J. Y. Back, T. K. An, Y. R. Cheon, H. Cha, J. Jang, Y. Kim, Y. Baek, D. S. Chung, S.-K. Kwon, C. E. Park, Y.-H. Kim, *ACS Appl. Mater. Interfaces* **2015**, *7*, 351.
- [34] S. Himmelberger, D. T. Duong, J. E. Northrup, J. Rivnay, F. P. V. Koch, B. S. Beckingham, N. Stingelin, R. A. Segalman, S. C. B. Mannsfeld, A. Salleo, *Adv. Funct. Mater.* **2015**, *25*, 2616.
- [35] X. Xu, Y. Yao, B. Shan, X. Gu, D. Liu, J. Liu, J. Xu, N. Zhao, W. Hu, Q. Miao, *Adv. Mater.* **2016**, *28*, 5276.
- [36] Z. Liang, Q. Tang, J. Xu, Q. Miao, *Adv. Mater.* **2011**, *23*, 1535.
- [37] X. Gao, C.-a. Di, Y. Hu, X. Yang, H. Fan, F. Zhang, Y. Liu, H. Li, D. Zhu, *J. Am. Chem. Soc.* **2010**, *132*, 3697.
- [38] J. Youn, S. Vegiraju, J. D. Emery, B. J. Leever, S. Kewalramani, S. J. Lou, S. Zhang, K. Prabakaran, Y. Ezhumalai, C. Kim, P.-Y. Huang, C. Stern, W.-C. Chang, M. J. Bedzyk, L. X. Chen, M.-C. Chen, A. Facchetti, T. J. Marks, *Adv. Electron. Mater.* **2015**, *1*, 1500098.
- [39] C. Zhang, Y. Zang, E. Gann, C. R. McNeill, X. Zhu, C.-a. Di, D. Zhu, *J. Am. Chem. Soc.* **2014**, *136*, 16176.
- [40] Q. Wu, X. Qiao, Q. Huang, J. Li, Y. Xiong, X. Gao, H. Li, *RSC Adv.* **2014**, *4*, 16939.
- [41] R. J. Chesterfield, C. R. Newman, T. M. Pappenfus, P. C. Ewbank, M. H. Haukaas, K. R. Mann, L. L. Miller, C. D. Frisbie, *Adv. Mater.* **2003**, *15*, 1278.
- [42] A. C. J. Heinrich, B. Thiedemann, P. J. Gates, A. Staubitz, *Org. Lett.* **2013**, *15*, 4666.
- [43] F. Gohier, P. Frère, J. Roncali, *J. Org. Chem.* **2013**, *78*, 1497.
- [44] Q. Wu, S. Ren, M. Wang, X. Qiao, H. Li, X. Gao, X. Yang, D. Zhu, *Adv. Funct. Mater.* **2013**, *23*, 2277.
- [45] Q. Wu, R. Li, W. Hong, H. Li, X. Gao, D. Zhu, *Chem. Mater.* **2011**, *23*, 3138.
- [46] M.-C. Chen, Y.-J. Chiang, C. Kim, Y.-J. Guo, S.-Y. Chen, Y.-J. Liang, Y.-W. Huang, T.-S. Hu, G.-H. Lee, A. Facchetti, T. J. Marks, *Chem. Commun.* **2009**, 1846.
- [47] C. Kim, M.-C. Chen, Y.-J. Chiang, Y.-J. Guo, J. Youn, H. Huang, Y.-J. Liang, Y.-J. Lin, Y.-W. Huang, T.-S. Hu, G.-H. Lee, A. Facchetti, T. J. Marks, *Org. Electron.* **2010**, *11*, 801.
- [48] Y. Liu, C.-a. Di, C. Du, Y. Liu, K. Lu, W. Qiu, G. Yu, *Chem. - Eur. J.* **2010**, *16*, 2231.
- [49] M.-C. Chen, S. Vegiraju, C.-M. Huang, P.-Y. Huang, K. Prabakaran, S. L. Yau, W.-C. Chen, W.-T. Peng, I. Chao, C. Kim, Y.-T. Tao, *J. Mater. Chem. C* **2014**, *2*, 8892.
- [50] I. Doi, E. Miyazaki, K. Takimiya, Y. Kunugi, *Chem. Mater.* **2007**, *19*, 5230.
- [51] S. Ukai, S. Igarashi, M. Nakajima, K. Marumoto, H. Ito, S. Kuroda, K. Nishimura, Y. Enomoto, G. Saito, *Colloids Surf., A* **2006**, *284–285*, 589.
- [52] T. Marszalek, A. Nosal, R. Pfattner, J. Jung, S. Kotarba, M. Mas-Torrent, B. Krause, J. Veciana, M. Gazicki-Lipman, C. Crickert, G. Schmidt, C. Rovira, J. Ulanski, *Org. Electron.* **2012**, *13*, 121.
- [53] X. Guo, R. P. Ortiz, Y. Zheng, M.-G. Kim, S. Zhang, Y. Hu, G. Lu, A. Facchetti, T. J. Marks, *J. Am. Chem. Soc.* **2011**, *133*, 13685.
- [54] S. C. Martens, U. Zschieschang, H. Wadepohl, H. Klauk, L. H. Gade, *Chem. - Eur. J.* **2012**, *18*, 3498.
- [55] B. A. Jones, M. J. Ahrens, M.-H. Yoon, A. Facchetti, T. J. Marks, M. R. Wasielewski, *Angew. Chem. Int. Ed.* **2004**, *43*, 6363.
- [56] J. H. Oh, S. Liu, Z. Bao, R. Schmidt, F. Würthner, *Appl. Phys. Lett.* **2007**, *91*, 212107.
- [57] R. Schmidt, M. M. Ling, J. H. Oh, M. Winkler, M. Könemann, Z. Bao, F. Würthner, *Adv. Mater.* **2007**, *19*, 3692.
- [58] H. A. Becerril, M. E. Roberts, Z. Liu, J. Locklin, Z. Bao, *Adv. Mater.* **2008**, *20*, 2588.
- [59] G. Giri, S. Park, M. Vosgueritchian, M. M. Shulaker, Z. Bao, *Adv. Mater.* **2014**, *26*, 487.
- [60] G. Giri, E. Verploegen, S. C. B. Mannsfeld, S. Atahan-Evrenk, D. H. Kim, S. Y. Lee, H. A. Becerril, A. Aspuru-Guzik, M. F. Toney, Z. Bao, *Nature* **2011**, *480*, 504.
- [61] Y. Diao, B. C. K. Tee, G. Giri, J. Xu, D. H. Kim, H. A. Becerril, R. M. Stoltenberg, T. H. Lee, G. Xue, S. C. B. Mannsfeld, Z. Bao, *Nat. Mater.* **2013**, *12*, 665.
- [62] J. H. Oh, W.-Y. Lee, T. Noe, W.-C. Chen, M. Könemann, Z. Bao, *J. Am. Chem. Soc.* **2011**, *133*, 4204.
- [63] S. Geib, U. Zschieschang, M. Gsänger, M. Stolte, F. Würthner, H. Wadepohl, H. Klauk, L. H. Gade, *Adv. Funct. Mater.* **2013**, *23*, 3866.